Geoderma 432 (2023) 116420

Contents lists available at ScienceDirect

Geoderma

journal homepage: www.elsevier.com/locate/geoderma

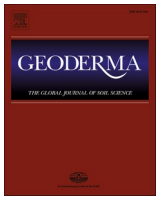

Relationship between thermal and electrical conductivity curves of soils with a unimodal pore size distribution: Part 1. A unified series-parallel resistor model

Lin Liu [a], Weiliu Li [a], Yili Lu [a], Tusheng Ren [a,*], Robert Horton [b]

[a] College of Land Science and Technology, China Agricultural University, Beijing 100193, China
[b] Agronomy Department, Iowa State University, Ames, IA 50011, USA

ARTICLE INFO

Handling Editor: Cristine L.S. Morgan

Keywords:
Thermal conductivity
Electrical conductivity
Series-parallel
Model
Porosity

ABSTRACT

Soil thermal conductivity (λ) and electrical conductivity (σ) characterize heat and electricity conduction through soils. Both λ and σ are affected by similar factors, such as soil water content (θ), texture, bulk density (ρ_b), temperature, structure, and organic matter content. Little is known about the quantitative relationship between λ and σ, and how soil texture and ρ_b modify the relationship. In this part one of a two-part series, we examine the correlation between λ(θ) and σ(θ) curves and develop a new model for normalized σ curves of soils with a unimodal pore size distribution. We introduce an Ohm's law analogy to describe the λ and σ curves conceptually, based on a cubic cell unit model. A unified series–parallel resistor model considering θ and ρ_b effects is established for both λ(θ) and σ(θ) curves by considering heat and electrical conduction pathways (solid, solid–liquid, and liquid pathways) in the hydration, menisci, and continuous liquid ranges. Simultaneous measurements of θ, λ and σ with thermo-TDR sensors on two soils are used to examine the model performance at various values of ρ_b and θ. The modeled and measured λ (θ) and σ (θ) curves provide consistent trends, and the normalized λ and σ values vs. degree of saturation confirm the existence of an earlier reported "mirror image" phenomenon between the functions.

1. Introduction

Soil thermal conductivity (λ), which measures the ability of a soil to conduct heat, is a vital parameter in heat transfer investigations (Farouki, 1986; Revil, 2000). Soil electrical conductivity (σ), which reflects the mobility of electrons in soils, is often used as an indirect indicator of soil physical and chemical properties, such as water content (θ), salinity and clay fraction (Sudduth et al., 2005; Stadler et al., 2015). Both λ and σ have been used to estimate soil physical properties, study surface energy balance and land–atmosphere interactions (Logsdon et al., 2010). Understanding the quantitative relationship between λ and σ is essential for predicting the coupling mechanisms of water, heat, and solute transport in soils.

Soil λ and σ are both affected by common factors such as θ, soil bulk density (ρ_b), mineral composition, particle size distribution and temperature (Nadler and Frenkel, 1980; Farouki, 1986; Logsdon et al., 2010). Inspired by the similarities between heat transfer and electrical flux in soils, some efforts have been made to reveal the interrelations between λ and σ. Woodside and Messmer (1961) studied soil heat transfer using a series–parallel resistor model following the theory of electrical flow in two-phase media. Revil (2000) proposed a theoretical λ model for saturated granular sediments, in which the pore topography effect was reflected by using an electrical cementation exponent that could be obtained from σ measurements. Hamamoto et al. (2010) studied λ, σ, and air/solute diffusivities under variably saturated fluid conditions and examined the analogies between the four parameters following an extended form of Archie's law. They proposed the "water bridge effect" (i.e., thermal conduction through the solid phase is enhanced as water content increases), "water blockage effect" (i.e., air diffusion decreases as water content increases), and "air blockage effect" (i.e., solute diffusion and electrical conduction decrease as air fraction increases) to describe the λ, σ, and air/solute diffusivities in response to the degree of water saturation (*S*). The analogies among the parameters showed a "mirror image" relationship between λ and σ using an extended form of Archie's second law (Hamamoto et al., 2010).

Some empirical equations have been developed to describe the λ-σ

* Corresponding author.
E-mail address: tsren@cau.edu.cn (T. Ren).

https://doi.org/10.1016/j.geoderma.2023.116420
Received 1 December 2022; Received in revised form 27 February 2023; Accepted 1 March 2023
Available online 7 March 2023

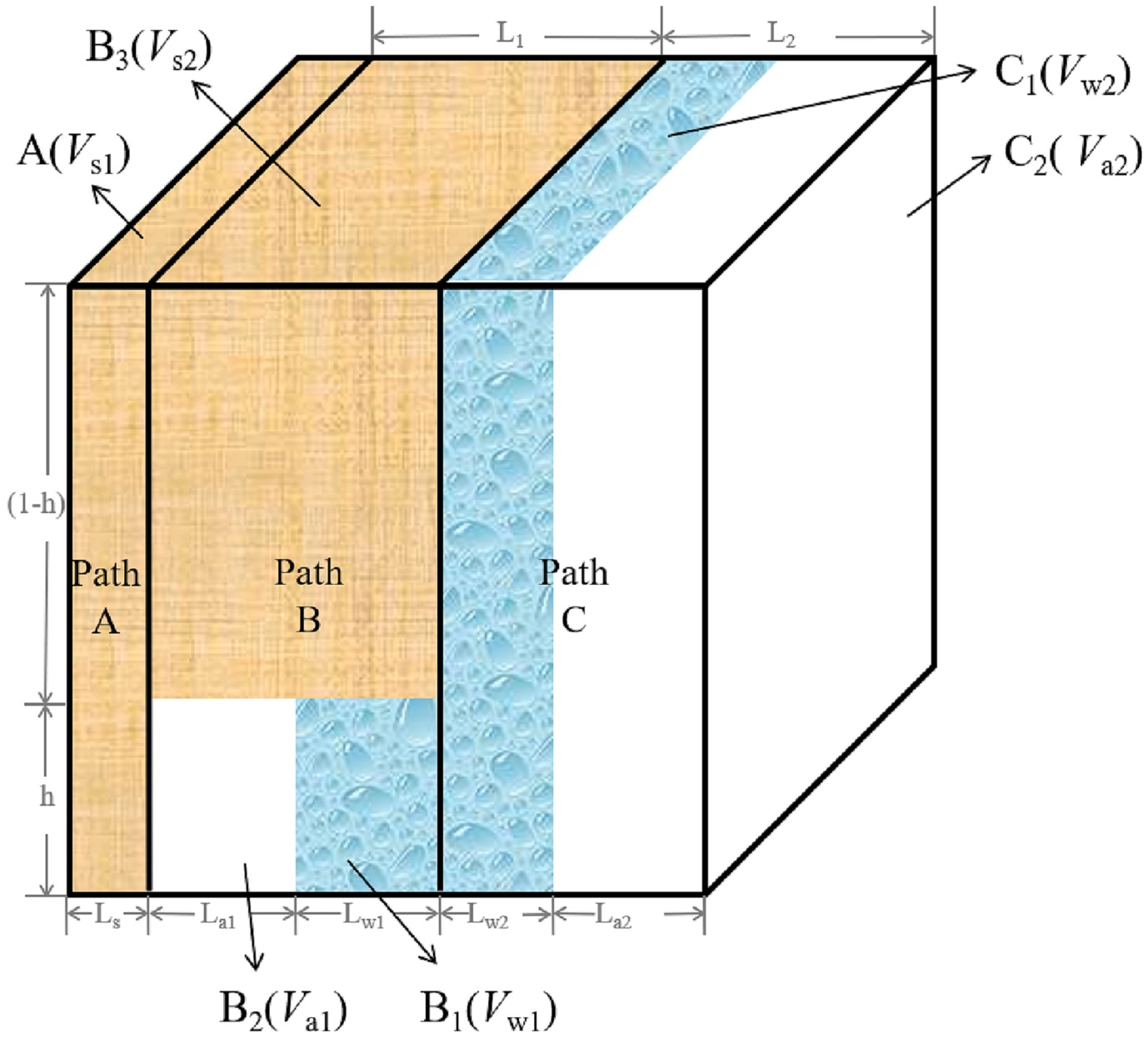

Fig. 1. A diagram of the soil cubic cell showing the unified series–parallel resistor model framework. Paths A, B, and C represent the solid contact path, the coupled path of solids and miniscule pores, and the continuous liquid path, respectively. In Path A, L_s is the horizontal length and V_{s1} is the corresponding volume. In Path B, the solid phase (B_3) and soil pores are arranged in series, soil liquid (B_1) and air (B_2) are arranged in parallel in the miniscule pores. W, L_{a1}, and L_{w1} are the horizontal lengths of solids, air, and liquid, respectively, and V_{s2}, V_{a1} and V_{w1} are the volumes of the corresponding components. In Path C, L_{a2} and L_{w2} are the horizontal lengths of air and liquid, respectively, and V_{a2} and V_{w2} are the volumes of the air and liquid paths, respectively.

relationships. Singh et al. (2001) proposed a general relationship between λ and electrical resistivity (1/σ). Sreedeep et al. (2005) further improved the model by including soil type and *S*. In geotechnical applications, Fragkogiannis et al. (2010) presented an empirical correlation for λ of subsurface soil based on 1/σ obtained from electrical tomography and geotechnical data. Wang et al. (2017) built a linear quantitative formula between λ and 1/σ by using a statistical analysis of observed λ-σ values. These λ-σ relationships are empirical and usually require soil-specific calibrations. There is a need for an in-depth investigation of the variations of λ or σ with soil type, θ, porosity (*n*), and eventually to establish a universal λ-σ relationship (Nouveau et al., 2016).

Several models have been established to estimate σ and λ from easily measurable soil properties and parameters. For soils with low θ values and solute concentrations, Rhoades et al. (1989) considered that electricity was conducted via three pathways acting in parallel in a cubic cell unit, including a solid pathway, a liquid pathway, and a solid–liquid series-coupled pathway. Because heat conduction and electrical conduction in partially saturated soils share similar pathways, Tarnawski and Leong (2012) modified and applied the cubic cell model to estimate λ of various soils. Tokoro et al. (2016) further studied the λ-θ model with the assumption that heat conduction in soils occurred mainly through three pathways. The advantage of the series–parallel resistor model is that it includes heat and electricity transport pathways through each soil phase, which makes it a useful tool for analyzing the physical mechanisms of heat and electrical conduction processes in soils.

Our objective in this study is to develop a unified model that describes λ and σ in response to θ and ρ_b values of partially saturated soils with a unimodal pore size distribution. In this Part 1 of a two-part series, we describe the unified series–parallel resistor model, which is

developed based on an Ohm's law analogy considering soil conductors (i.e., soil solid, liquid and air) acting in parallel or in series in a cubic cell unit. The model is then used to explore how the mechanisms of λ and σ change with θ for soils of various texture and ρ_b. A laboratory experiment is performed to verify the model results. Finally, a new normalized σ model is derived from the Lu et al. (2007) λ model based on the "mirror image" relationship between λ and σ.

2. Development of the unified series-parallel resistor model

The unified series-parallel resistor model is applied to investigate the relationship between λ-θ and σ-θ curves. The proposed model framework is built on the concept of a cubic cell unit that has been used by Tarnawski and Leong (2012) to model λ variations with soil texture, with the assumption that (1) the soil has a unimodal particle size distribution; (2) there are similarities between heat conduction and electricity conduction in soils, and (3) both processes can be quantified with the cubic cell unit setting.

The cubic cell unit includes three separate components (Fig. 1), representing the solid phase (yellow section), air phase (blank section) and liquid phase (blue section). In the cubic cell model, heat conduction and electrical conduction occur via three pathways arranged in parallel, i.e., solid-to-solid contacts (Path A), a coupled pathway of miniscule pores (miniscule portion of soil water and air arranged in parallel) and solids (Path B), and a continuous liquid pathway (Path C). In Path A, heat and electrical conductions occur only through the solids or the surface of solid particles (i.e., surface conductance). In Path B, the solid phase (B_3) and soil pores are arranged in series in the miniscule pores, and soil liquid (B_1) and soil air (B_2) are arranged in parallel. The pores included in Path C consist of continuous liquid (C_1) and air (C_2), which are arranged in parallel.

For simplification of model development, the side length of the cubic cell unit is assumed to be 1 (dimensionless) (Fig. 1). The dimensionless horizontal lengths of Paths A, B and C are denoted as L_s, L_1, and L_2, respectively. The dimensionless horizontal lengths of soil air and liquid in Path B are indicated by L_{a1} and L_{w1}, respectively, and in Path C by L_{a2} and L_{w2}, respectively. The terms h and (1-h) are the vertical lengths of the soil liquid/air and the vertical length of the solids in Path B, respectively, which are coupled in series (Fig. 1). These side lengths can be varied to reflect the different ratios of solids, liquid, and air in the cubic cell unit. According to Fig. 1, the corresponding volumes of A, B_3, B_1, B_2, C_1, and C_2 are V_{s1}, V_{s2}, V_{w1}, V_{a1}, V_{w2}, and V_{a2}, respectively. It should be noted that the volumes defined here simply represent the apparent sizes involved in heat and electrical conductions within the cubic cell unit, not the actual volume of the physical soil.

Following an Ohm's Law analogy, the electrical or thermal resistance (R) through the cubic cell unit is,

$$R = \frac{L}{cA} \tag{1}$$

where L is the electrical and heat conduction length through the conduit, c represents either apparent λ or σ, A is the cross-sectional area of the heat or electricity conduction path.

By applying Eq. [1] to each component within the cubic cell unit, the electrical or thermal resistance of each path in Fig. 1 is derived,

$$R_{V_{s1}} = \frac{1}{c_s L_s} \tag{2}$$

$$R_{V_{s2}} = \frac{1-h}{c_s L_2} \tag{3}$$

$$R_{V_{w1}} = \frac{h}{c_w L_{w1}} \tag{4}$$

$$R_{V_{a1}} = \frac{h}{c_a L_{a1}} \tag{5}$$

$$R_{V_{w_2}} = \frac{1}{c_w L_{w_2}} \tag{6}$$

$$R_{V_{a2}} = \frac{1}{c_a L_{a2}} \tag{7}$$

where c_s, c_w, and c_a represent the thermal or electrical conductivities of soil solids, liquid, and air, respectively.

Based on Eqs. [2]-[7], a unified series–parallel resistor model for λ(θ) and σ(θ) is proposed. In the model scheme, we differentiate soil water into three water content ranges by considering the interactions of water with soil solids: (1) the hydration range, where water is adsorbed on the surface of solid particles, (2) the menisci range, where water bridges are formed between soil particles (from maximum adsorbed water up to the point where a continuous liquid pathway is formed), and (3) the continuous liquid range, where liquid water replaces air steadily until saturation is achieved. For model development, we assume that as θ increases (e.g., during a wetting process), water is adsorbed onto solid particles first, then fills in the relatively smaller pores in Path B, and finally enters the larger pores in Path C. Within each water range, the apparent electrical or thermal resistance (R_a) of the cubic cell unit is derived. Therefore, the unified series–parallel resistor model is represented by a piecewise function according to the three water content ranges.

In the hydration range, water is adsorbed on soil particles by hydrogen bonding or intermolecular forces due to Van der Waals forces (Lu and Dong, 2015). The θ value ranges between zero and the maximum adsorbed water content (θ_{ads}), and $L_{a1} = L_1$, $L_{w1} = L_{w2} = 0$, $L_{a2} = L_2$. In this range, the adsorbed water hardly affects the λ or σ values. Thus, the electrical or thermal resistivity is,

$$\frac{1}{R_a} = \frac{1}{R_{V_{s1}}} + \frac{1}{R_{V_{s2}} + R_{V_{a1}}} + \frac{1}{R_{V_{a2}}}, 0 \leqslant \theta \leqslant \theta_{ads} \tag{8}$$

In the menisci range, water fills in the miniscule pores gradually. As θ increases, L_{a1} decreases and L_{w1} increases gradually while L_2 remains unchanged. At the point of $L_{a1} = 0$, the miniscule pores (i.e., the total pore volume of Paths B_1 and B_2, n_{wm}, $L_1 h$) are filled completely with water. We define this water content as θ_c, which equals to the sum of θ_{ads} and n_{wm}. Thus, in the menisci range, θ varies from θ_{ads} to θ_c, and R_a is represented by,

$$\frac{1}{R_a} = \frac{1}{R_{V_{s1}}} + \frac{1}{R_{V_{s2}} + \frac{1}{\frac{1}{R_{V_{a1}}} + \frac{1}{R_{V_{w1}}}}} + \frac{1}{R_{V_{a2}}}, \theta_{ads} < \theta \leqslant \theta_c \tag{9}$$

In Path C, as θ is further increased, continuous water steadily replaces air in larger pores. During this process, L_{a2} decreases gradually while L_{a1} and L_{w1} remain constant. Thus, the R_a of the continuous liquid range ($\theta_c < \theta \leq n$) is calculated with,

$$\frac{1}{R_a} = \frac{1}{R_{V_{s1}}} + \frac{1}{R_{V_{s2}} + R_{V_{w1}}} + \frac{1}{R_{V_{a2}}} + \frac{1}{R_{V_{w2}}}, \theta_c < \theta \leqslant n \tag{10}$$

Equations [8]-[10] form the unified series–parallel resistor model for soil electrical and thermal resistivities. The individual terms of the model are defined in Eqs. [2]-[7].

It is evident that by defining the physical length for each transport path, the unified series–parallel model developed here has extended the Tarnawski and Leong (2012) λ model, and it describes the λ and σ curves simultaneously and quantitatively. This provides a useful way to investigate the relationship between λ and σ and the coupled transport of heat and solutes in soils.

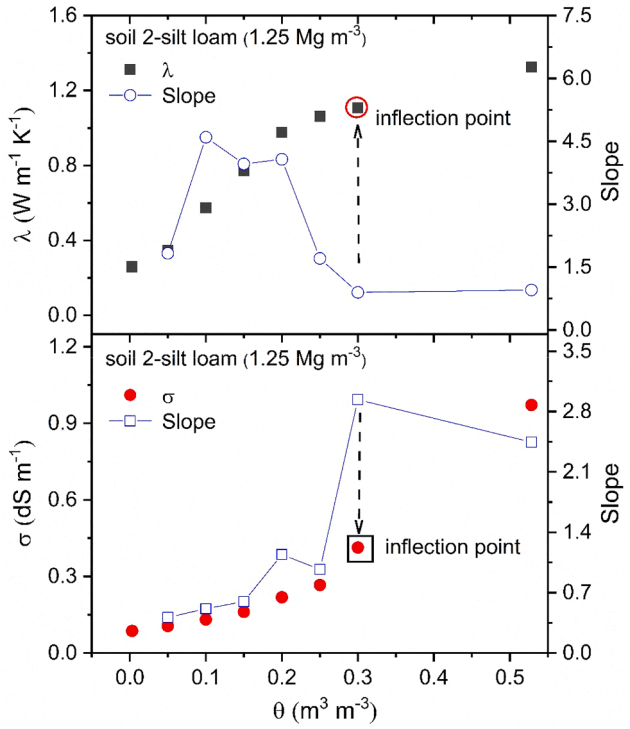

Fig. 2. Determination of the inflection point of thermal conductivity (λ) and electrical conductivity (σ) using the slopes of the λ(θ) or σ(θ)curves. Here soil 2 (a silt loam) is used as an example.

3. Assumptions and parameterization of the unified series–parallel resistor model

In this section, we present the model assumptions and the parameterization procedures for generating λ and σ curves of two hypothetical soils H1 and H2 with different textures.

3.1. Assumptions of the unified series–parallel model

Following the model framework defined in Fig. 1, the volume of each soil component is defined based on the following assumptions:

(1) The soils are classified into fine-texture and coarse-texture groups using a sand fraction (f_{sa}) of 0.40 following Lu et al. (2007). Compared to fine-texture soils ($f_{sa} \leq 0.40$), coarse-texture soils ($f_{sa} > 0.40$) have a larger proportion of pores in Path C, and a smaller proportion of miniscule pores in Path B. Miniscule pores are those having water meniscus between soil particles (Clapp and Hornberger, 1978; Campbell, 1985; Tarnawski and Leong, 2012).

(2) During the wetting process, water first fills in relatively small soil pores (Path B) and then enters the larger pores (Path C).

(3) Some cation exchanges occur between the solid and liquid phases over the entire range of water content. According to Waxman and Smits (1968), at a specified saturation, the effective concentration of exchangeable ions was a linear function of the saturation and the concentration of exchangeable ions. Thus, the σ_w value at a specified saturation (σ_w') is expressed as the product of S and the σ_w at saturation,

$$\sigma_w' = \sigma_w S \quad (11)$$

Thus, parameter c_w in Eqs. [4] and [6] is replaced by σ_w' when calculating the σ values.

3.2. Parameterization of the unified series–parallel model

Model parameters (θ_{ads}, θ_c, c values of soil solids, air and liquid, and side lengths) are determined with the purpose of obtaining the cubic cell unit, which represents soils of various textures, θ and ρ_b. For θ_{ads}, the values from Lu et al. (2018) are used (Table A1 in Appendix A), i.e., the θ_{ads} value is set as 0.01 $m^3\ m^{-3}$ for soil H1 (sand) and 0.08 $m^3\ m^{-3}$ for soil H2 (silt loam).

The parameter θ_c represents the inflection point of the λ(θ) and σ(θ) curves, which corresponds to the peak slope of λ versus θ and the dip in the σ versus θ, which equals the sum of θ_{ads} and n_{wm} in our model. As an example, for soil 2, according to the change rates of λ and σ with θ (details of λ and σ measurements are described in Part 2), the two curves have approximately the same θ_c value of 0.30 $m^3\ m^{-3}$ (Fig. 2).

The apparent thermal and electrical conductivity values (i.e., the c value in Eq. [1]) of soil solids, air, and liquid are obtained from the literature (Appendix B). For soils H1 and H2, the λ_a, λ_w, and σ_a values are set as 0.025, 0.56 W m^{-1} K^{-1}, and 0.0001 dS m^{-1}, respectively (de Vries, 1963; McNeill, 1980; Palacky, 1987; Tarnawski and Leong, 2012); the σ_s and σ_w values are set as 0.025 and 0.40 dS m^{-1} for soil H1, and 0.08 and 3.00 dS m^{-1} for soil H2 (Palacky, 1987). By considering the influences of the quartz content (Table 1), the calculated λ_s values are 6.82 and 3.16 W m^{-1} K^{-1} for soils H1 and H2, respectively (Johansen, 1975).

The desired ρ_b ranges for the two soils are determined by altering the length parameters W, L_2, L_s and h in the cubic cell unit (Fig. 1). For soils H1 and H2, the ρ_b ranges from 1.15 to 1.60 Mg m^{-3}, and the side lengths are calculated accordingly using the procedures listed in Appendix C. Finally, the proper values for L_1, L_2 and h are obtained (Fig. C9). Table 1 presents a summary of the specific properties and length parameters of the two hypothetical soils. For soil H1, L_s, L_1, L_2, and h are in the ranges of 0.01–0.01, 0.58–0.65, 0.34–0.41, and 0.07–0.09, respectively, and the corresponding values for soil H2 are in the ranges of 0.03–0.04, 0.58–0.65, 0.31–0.39, and 0.15–0.17, respectively (Table 1).

Fig. 3 outlines the procedures for obtaining soil λ and σ curves by using the unified series–parallel resistor model.

4. Results and discussion

In this section, we present the results from the unified series–parallel resistor model as well as the measurements representing four soils at various θ and ρ_b values. The effects of soil texture, θ, and ρ_b on the λ and σ curves and the analogy between λ and σ are discussed.

Table 1
The input parameters of the series–parallel resistor model for two hypothetical soils (H1 and H2) with different textures and bulk densities (ρ_b). Parameters λ_s, λ_w, σ_s, and σ_w are the thermal and electrical conductivities of solid and liquid, h, L_s, L_1, L_2 are the length parameters of the cubic cell model and n is the total porosity.

Soil ID	Texture	λ_s	λ_w	σ_s	σ_w	h	L_s	L_1	L_2	n	ρ_b
		W m^{-1} k^{-1}		dS m^{-1}		dimensionless					Mg m^{-3}
H1	sand	6.82	0.56	0.025	0.40	0.09	0.01	0.58	0.41	0.47	1.40
						0.09	0.01	0.62	0.37	0.43	1.51
						0.07	0.01	0.65	0.34	0.40	1.60
H2	silt loam	3.16	0.56	0.040	3.00	0.18	0.03	0.58	0.39	0.57	1.14
						0.16	0.04	0.62	0.34	0.53	1.26
						0.15	0.04	0.65	0.31	0.49	1.36

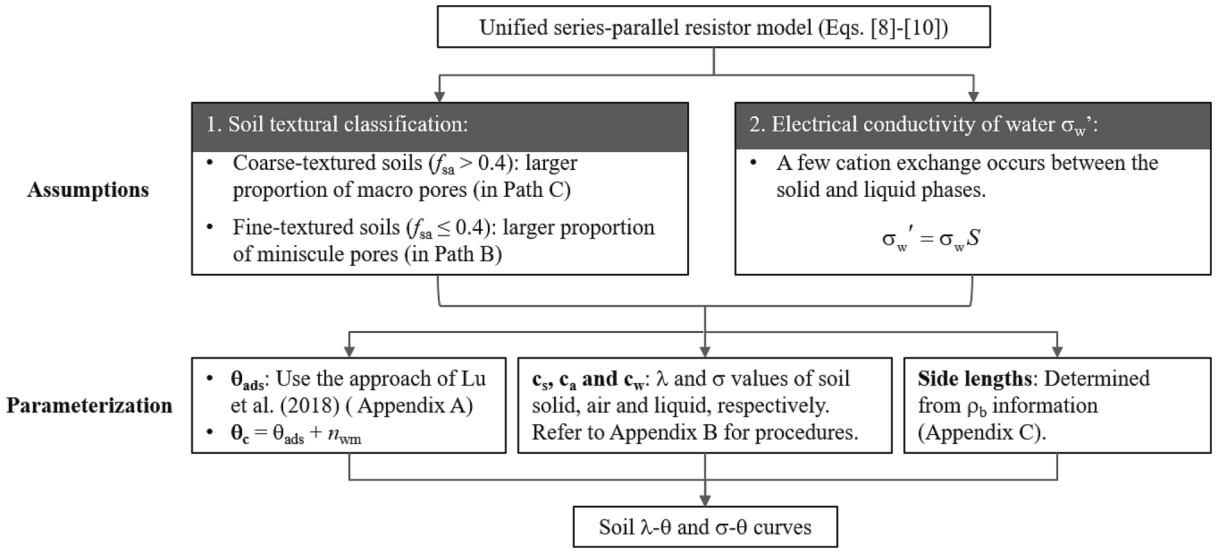

Fig. 3. Procedures to obtain soil thermal conductivity (λ) and electrical conductivity (σ) curves in the unified series–parallel resistor model. Parameters c_s, c_a and c_w are the λ and σ values of soil solids, air, and liquid, f_{sa} is sand fraction, σ_w' is σ_w at a specific saturation (S), ρ_b is soil bulk density, n_{wm} is volumetric fraction of miniscule pores, and θ_{ads} and θ_c are the maximum adsorbed and critical water contents of the λ and σ curves, respectively.

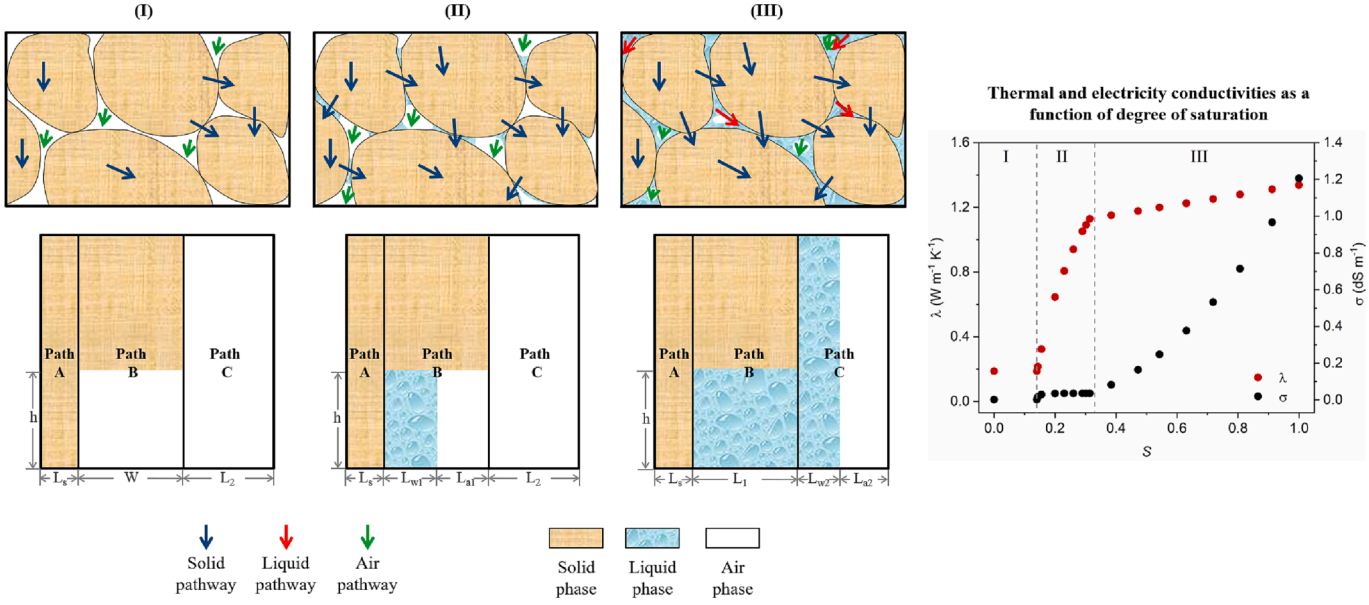

Fig. 4. A conceptual diagram showing heat and electrical conduction mechanisms in soils at different water content ranges (left). Three scenarios, i.e., hydration range (I), menisci range (II), and continuous liquid range (III), are considered. On the right, we show the thermal conductivity (λ)and electrical conductivity (σ)of soil H2 as a function of degree of water saturation (S) estimated with the unified series–parallel resistor model. The length parameters of soil H2 are included in Table 1.

4.1. Variations of λ and σ with S: the unified series-parallel resistor model

Fig. 4 displays the conceptual mechanisms for heat and electrical conduction in soil. The heat and electrical fluxes are set downwards. The blue, green, and red arrows represent the conduction pathways in solid, air, and liquid phases, respectively. The λ and σ curves of soil H2, which are obtained by using the unified model, are also included.

Heat and electrical conduction mechanisms and the associated λ and σ characteristics differ in the hydration, menisci, and continuous liquid ranges.

In the hydration range ($0 \le \theta \le \theta_{ads}$), water molecules are adsorbed onto the soil solid particle surfaces due to intermolecular forces such as van der Waals forces, cations (e.g., sodium and calcium), anions (i.e., oxygen anion or hydroxyls) or hydrogen bond of water (Lu and Dong, 2015). As a result, heat conduction within this range occurs only through the solid pathway (Path A), leading to extremely low λ values that are similar in value to those for dry soils (λ_{dry}), and in this range the values hardly change with θ (Section I in Fig. 4). Meanwhile, little change in σ is observed because electrical current flows mainly through the contacts of solid particles and along the surfaces of the soil solids (surface conductance), which essentially equals to the electrical conductivity of dry soils (σ_{dry}). In this range, both λ and σ values are related to L_S that controls the volume fraction of soil solids in Path A.

The transition between the hydration range and the menisci range occurs at the maximum adsorption water content (θ_{ads}) where all of the soil particles are coated with an adsorbed water film (Fig. 4). Additional water, which is reflected by h and L_{w1} in the unified series–parallel model, starts to form 'water bridges' between soil particles (Ewing and

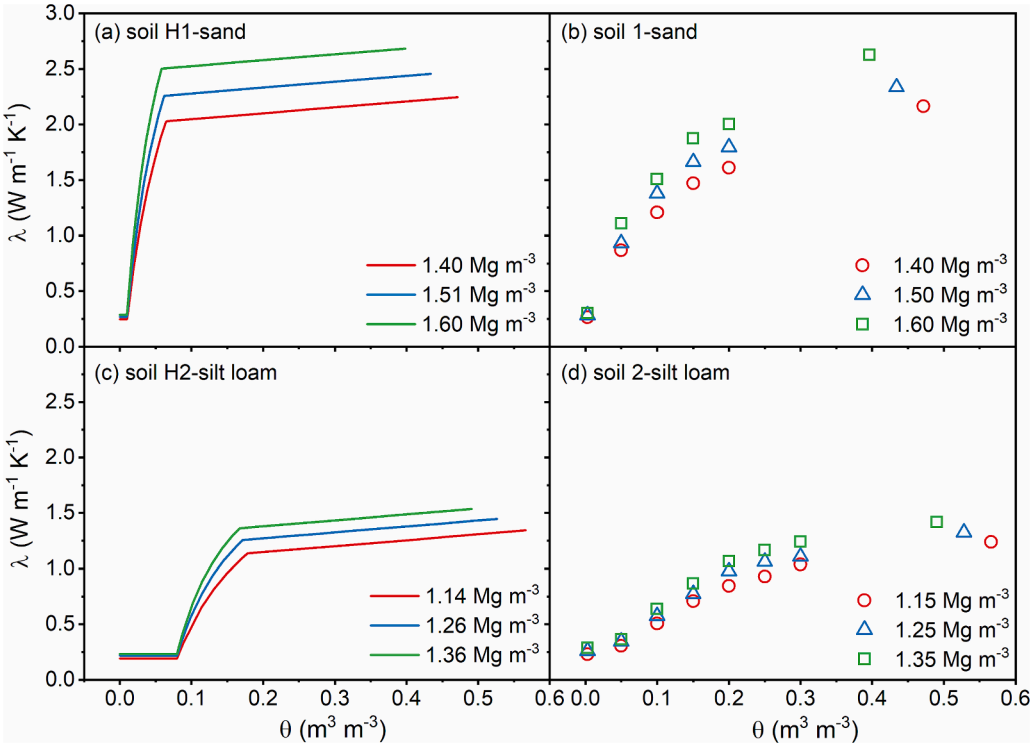

Fig. 5. Soil thermal conductivity (λ) versus water content (θ) for a set of bulk density values of a sand soil and a silt loam soil. Series-parallel resistor model estimates are shown in (a and c), and observed values are presented in (b and d). The length parameters of the hypothetical soils are provided in Table 1, and the physical properties of soils 1 and 2 are listed in Table 1 of Part 2 of the series.

Horton, 2007). These water bridges significantly enhance heat conduction efficiency through solid particles (Path B, which dominates over Path A) because heat transfer paths through the bridge-connected particles are increased dramatically with the rapid expansion of particle-to-particle contact area. As a result, a sharp λ increase with *S* is observed (Section II in Fig. 4). In contrast, only a slight σ change with *S* is observed because electrical conduction is constrained in the solid pathway (Path A) and solid–liquid pathway (Path B), and the soil solids have extremely weak electrical conduction ability (Rhoades et al., 1989). Thus, in the menisci water range ($\theta_{ads} < \theta \leq \theta_c$), the interaction between water and soil solids enhances heat conduction significantly but has limited improvement on electrical conduction, which leads to a rapid λ increase but a very slow σ change with *S* in Section II (Fig. 4).

With a further increase in *S* (i.e., $\theta > \theta_c$), the miniscule pores are filled with water completely (i.e., L_{w1} reaches the maximum fraction) and additional water starts to replace air in large pores (L_{w2} increases and L_{a2} decreases), which forms the continuous liquid pathways for heat and electrical conduction (Fig. 4). As a result, all the pathways (i.e., the solid, solid–liquid, and liquid pathways) contribute to heat conduction and electron transfer. In this range, however, the responses of λ and σ differ considerably to *S* increases with the formation of a continuous liquid pathway (Section III of Fig. 4). Since the change of λ is due mainly to the replacement of air with liquid, and λ_w is only 10–20% of λ_s, a steady and linear λ increase with *S* occurs (Lu et al., 2007; Lu et al., 2014), but with a lower rate of change as compared to those in Stage II. In contrast, a sharp σ increase with *S* occurs because the value of σ_w is 6–8 times larger than that of σ_s (Table 1).

4.2. The λ curves: observed values vs. unified series–parallel model results

Fig. 5 presents the estimated λ values for two hypothetical soils with ρ_b values ranging from 1.14 to 1.61 Mg m^{-3}, along with observed values from two actual soils with similar texture and bulk density as the hypothetical soils. The details for the observations are described in Part 2 of the series.

In general, the unified series–parallel resistor model captured the general trend of λ as a function of θ. Regardless of soil texture, λ values were relatively small and showed little variation in the hydration range, increased with a large slope in the menisci range, and increased further but with a small slope in the continuous liquid range. The model estimated values at the dry and saturated states were similar to the observed values, and the characteristic water content θ_{ads} in the λ(θ) curves approximated the observations, indicating that the Johansen (1975) model and Lu et al (2018) model provided reliable λ_s and θ_{ads} values, respectively.

4.2.1. Soil texture effects on λ(θ) curves

The unified series–parallel resistor model depicted well the effects of soil texture on λ. Compared to the silt loam soil results, the sand soil (1) had a smaller amount of hydration water due to the low specific surface area and limited electrical charges, which led to an earlier transition (i.e., a smaller θ_{ads} value) from the hydration range to the menisci range; (2) had a relatively small fraction of fine pores, thus the solid particles were readily connected by water molecules in the menisci water content range, resulting in a sharp λ response to a θ increase (Fig. 5a and 5b). Due to its large specific surface area, abundant electrical charges, and a high fraction of fine pores, the silt loam soil had a broader hydration range (i.e., greater θ_{ads} value) and a relatively small λ change rate with θ increase in the menisci water range (Fig. 5c and 5d), as compared to that of the sand soil.

4.2.2. ρ_b effects on λ(θ) curves

At a specific water content, a larger ρ_b value generally results in a greater λ value (Abu-Hamdeh and Reeder, 2000; Lu et al., 2014). Soils with large ρ_b values have a large soil solid fraction and better contacts among the solid particles, which offer heat conduction pathways through the bulk soil (Logsdon et al., 2010; Sun and Lü, 2019). The series–parallel resistor model results and the observations confirmed

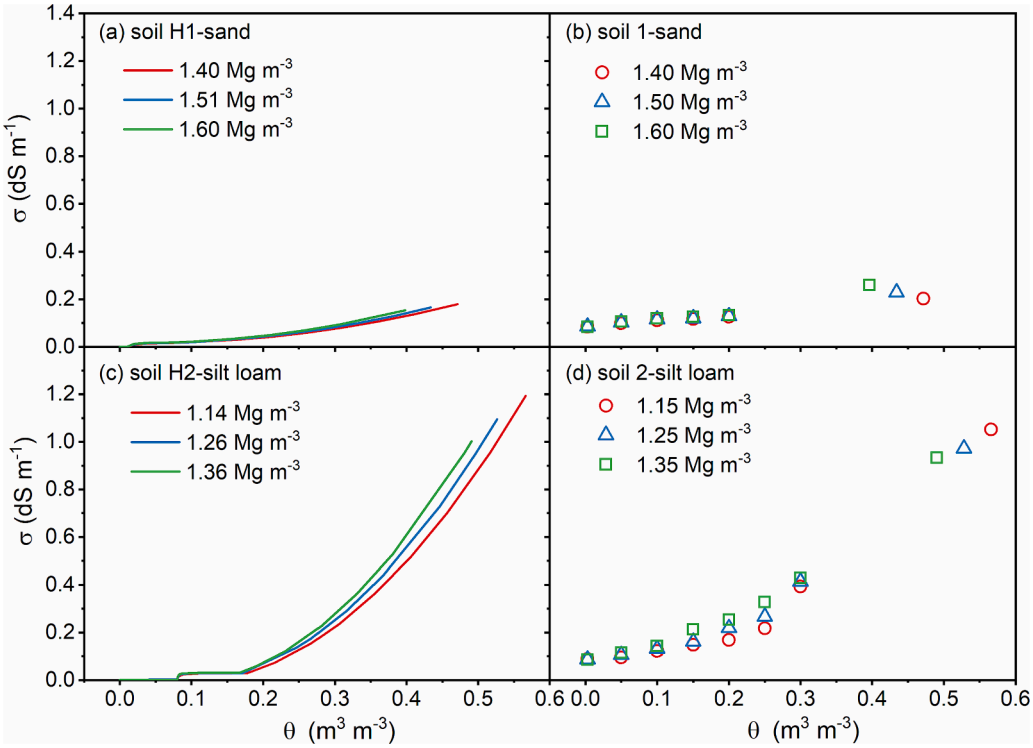

Fig. 6. Soil electrical conductivity (σ) versus water content (θ) at several values of bulk density for a sand soil and a silt loam soil. Presented are series–parallel resistor model estimations (a and c) and observed values (b and d). The length parameters of the hypothetical soils are shown in Table 1 and the physical properties of actual soils 1 and 2 are listed in Table 1 of Part 2 of the series.

Table 2
Electrical conductivity values for dry soil (σ_{dry}) and for saturated soil (σ_{sat}), and thermal conductivity values for dry soil (λ_{dry}) and for saturated soil (λ_{sat}) representing various textures and bulk densities (ρ_b).

Soil ID	Texture	ρ_b	σ_{dry}	σ_{sat}	λ_{dry}	λ_{sat}
		Mg m^{-3}	dS m^{-1}		W m^{-1} K^{-1}	
1	sand	1.40	0.08	0.20	0.24	2.16
		1.50	0.09	0.23	0.27	2.34
		1.60	0.08	0.26	0.29	2.62
2	silt loam	1.15	0.09	1.05	0.23	1.24
		1.25	0.08	0.97	0.26	1.32
		1.35	0.08	0.94	0.29	1.42
H1	sand	1.40	0.001	0.18	0.23	2.27
		1.51	0.001	0.16	0.27	2.52
		1.60	0.001	0.15	0.30	2.74
H2	silt loam	1.14	0.001	1.20	0.19	1.34
		1.26	0.002	1.05	0.22	1.41
		1.36	0.002	0.96	0.24	1.51

these findings and revealed that the responses of the λ(θ) curves to ρ_b varied with soil water content. The effect of ρ_b occurred mainly in the hydration and menisci water ranges where heat transfer through soil particles is the dominant mode. Taking soil H1 as an example, in the hydration range ($0 \le \theta \le \theta_{ads}$), a 6.7% increase in ρ_b produced a λ increase of 0.035 W m^{-1} K^{-1} (or a relative λ change of 13.5%). In this range, λ values increased with ρ_b because of greater contact areas (and thus a larger Path A) among the compacted solid particles. The λ increase, however, was small due to a limited number of disconnected heat conduction pathways.

As θ increases, the less conductive air phase is displaced by a more conductive liquid phase filling the miniscule pores (path B), which forms continuous solid–liquid pathways. For a particular soil, a larger ρ_b brings about a greater proportion of miniscule pores in total pore space (n_{wm}/n) and a greater proportion of solids, which forms additional conductive solid–liquid pathways and finally produces a greater inflection point between Section II and Section III. Therefore, in this range, λ increases appear at elevated ρ_b values. The largest relative λ change occurred at the water content (θ_i) where 'water bridges' first formed. From θ_{ads} to θ_i, a 6.7% increase in the ρ_b value resulted in a λ increase of 0.035–0.25 W m^{-1} K^{-1} (or a relative λ change from 13.5% to 17.8%). In the water content range from θ_i to θ_c, a 6.7% increase in the ρ_b resulted in a λ increase of 0.25–0.26 W m^{-1} K^{-1} (or a relative λ change from 17.8% to 11.9%).

When the soil solids are completely connected by 'water bridges', the λ(θ) curve enters the continuous liquid range ($\theta_c < \theta \le n$), where a 6.7% ρ_b increase caused a steady λ increase of 0.26 W m^{-1} K^{-1} (with a relative λ change of about 10.2%) throughout the continuous liquid pathway section (Path C).

While the λ(θ) curves produced by the unified model matched observed values reasonably well, some deviations were observed between the modelled and measured λ data (Fig. 5). First, compared to the observations, the λ(θ) curves derived from the unified model displayed a sharper inflection point, and the curves had different slopes at some ρ_b values. This is caused by the fact that the unified model ignores the gradual evolution of pore size and soil structure effects on heat conduction. Second, in the continuous liquid range, the λ increase caused by elevated ρ_b values in the series–parallel model were insensitive to θ changes, while larger λ values occurred at larger θ values in the observations. The root of this discrepancy is the model assumption that water first fills relatively small soil pores (Path B) and then enters the larger pores (Path C). Thus, in Path C, λ changes due to elevated ρ_b values related only to L_1, L_2, and h, and were not sensitive to θ changes (Appendix D). In practice, some macropores might be filled with water prior to the miniscule pores (Tarnawski and Leong, 2012). Future studies are required to further improve the model.

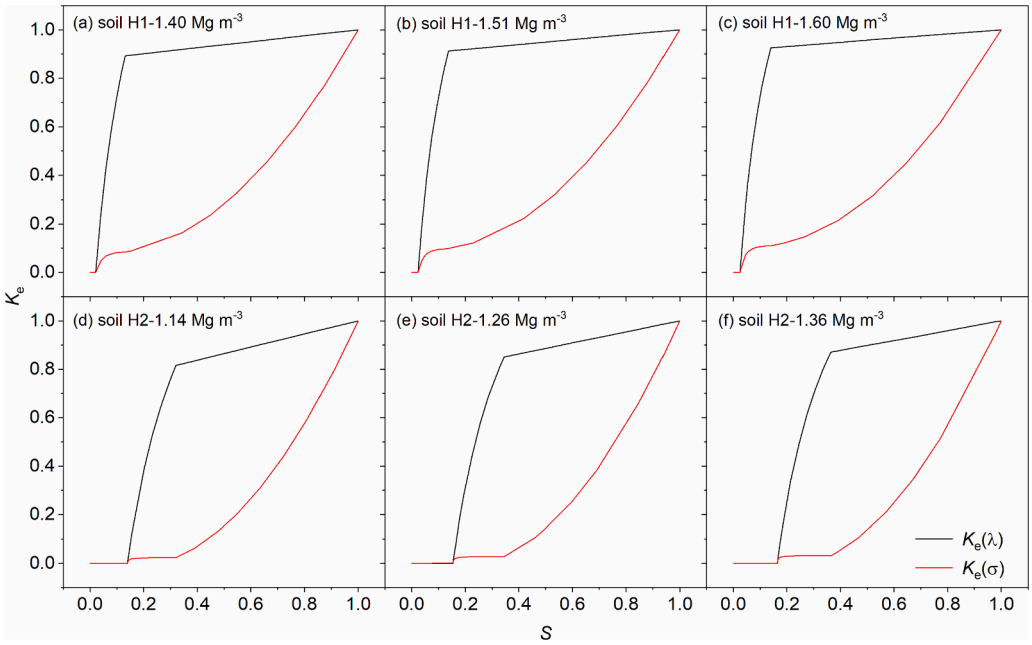

Fig. 7. Normalized series–parallel resistor model values (K_e) of soil thermal conductivity (λ) and bulk electrical conductivity (σ) versus degree of saturation (S) for a sand soil (H1) and a silt loam soil (H2) at selected values of bulk density.

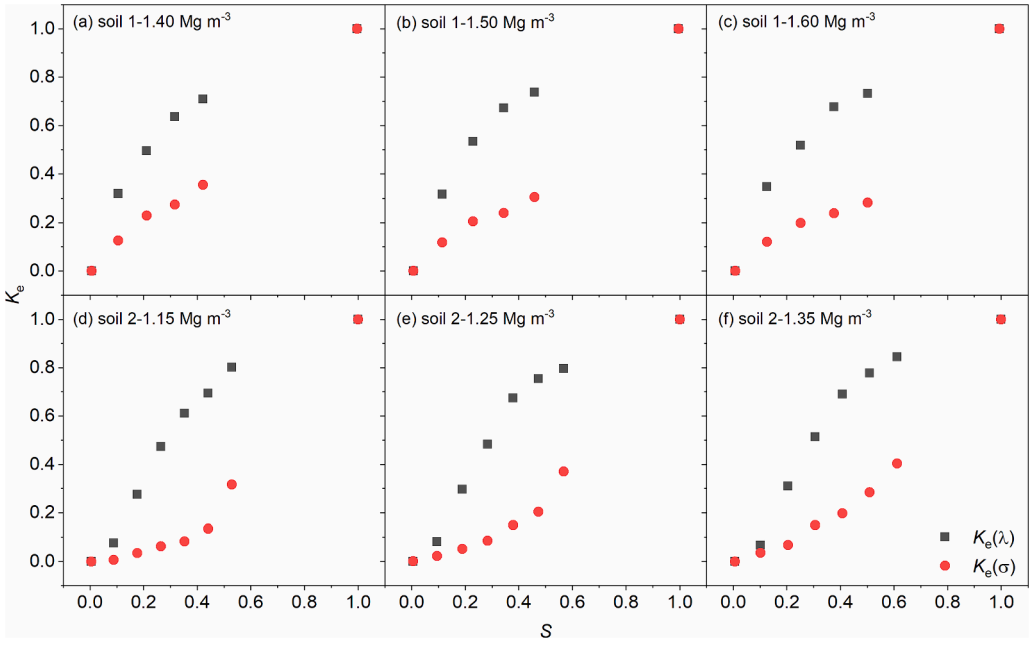

Fig. 8. Normalized values (K_e) of measured soil thermal conductivity (λ) and bulk electrical conductivity (σ) versus degree of saturation (S) for a sand soil (soil 1) and a silt loam soil (soil 2) at selected values of bulk density.

Table A3
The maximum adsorbed water content (θ_{ads}) for different soil textures. The values are from Lu et al. (2018).

Soil texture	θ_{ads} ($m^3\ m^{-3}$)
Sand	0.01
Sandy loam	0.04
Loam	0.03
Silt loam	0.08
Clay loam	0.10
Silty clay loam	0.09
Silty clay	0.14

4.3. The σ (θ curve: observed values vs. unified series–parallel model results

Fig. 6 presents the estimated σ(θ) curves of two hypothetical soils with ρ_b values ranging from 1.14 to 1.61 Mg m^{-3}, along with observations from two actual soils with similar textures and bulk densities as the hypothetical soils. The measurement details for the observations are described in Part 2 of the series.

Regardless of soil texture, σ values were small and did not vary much in the hydration range, increased slowly in the menisci range, and grew rapidly in the continuous liquid water range, indicating that the unified

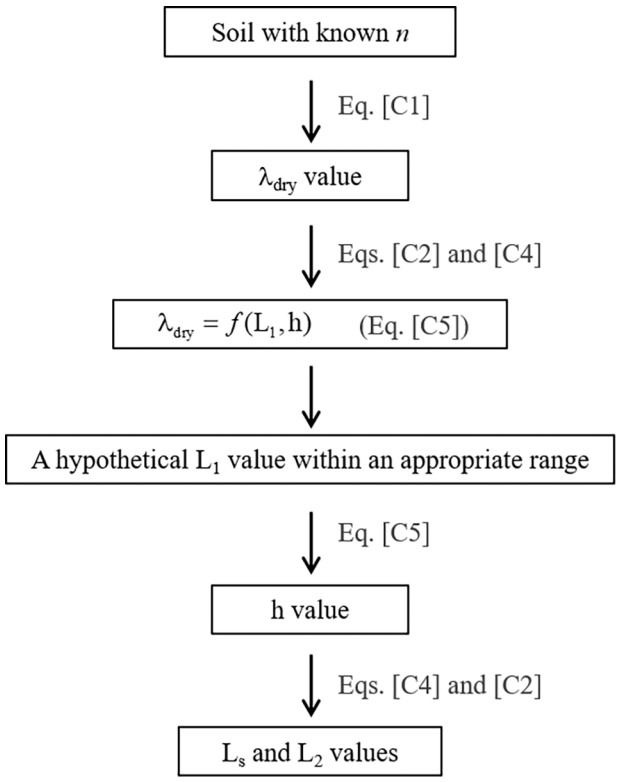

Fig. C1. The detailed procedure used to determine parameters L_s, h, L_1, and L_2. n is the total porosity, and λ_{dry} is thermal conductivity of dry soil.

series–parallel resistor model captured the overall trend of the σ versus θ relationship.

4.3.1. Soil texture effects on σ(θ) curves

Compared to the silt loam soil, the sand soil had less hydration water due to the low specific surface areas and limited electrical charges, which led to an earlier transition (i.e., a lower θ_{ads} value) from the hydration range to the menisci range. Due to a large specific surface area, abundant electrical charges, and a high fraction of fine pores, the silt loam soil had a broader hydration range (i.e., greater θ_{ads} value) and a relatively large σ versus θ slope in the continuous liquid range (Fig. 6c and 6d), as compared to that of the sand soil. Thus, the unified series–parallel resistor model was able to capture soil texture effects on σ.

4.3.2. ρ_b effects on σ(θ) curves

It is accepted that for a given soil, larger ρ_b results in larger σ values at the same θ (Logsdon et al., 2010). The series–parallel resistor model results and the observations not only confirmed these findings, but also revealed that the response of the σ(θ) curves to ρ_b varied with soil water content, in a way similar to that of the λ(θ) curves: (1) At a specific θ, greater σ values were observed at elevated ρ_b values; and (2) σ increases with ρ_b occurred mainly in the menisci stage where the solid–liquid pathway dominated electrical conduction. Taking soil H1 as an example, in the hydration range ($0 \le \theta \le \theta_{ads}$), electrical current flows mainly through the discontinuous solid-to-solid pathway, and the influence of elevated ρ_b on σ values was negligible because of the extremely low σ_s values.

In the menisci range ($\theta_{ads} < \theta \le \theta_c$), water molecules in the pores form 'water bridges' among soil solids, allowing electricity to be conducted mainly in the solid-to-solid pathway (Path B). Thus, from θ_{ads} to θ_i, a significant ρ_b effect on σ was observed: A 6.7% ρ_b increase caused a σ increase of 0–0.80 × 10^{-3} dS m^{-1} (or a relative σ change from 0.4% to 28.1%). As θ further increased, 'water bridges' increased, and σ varied from 0.80 to 2.65 × 10^{-3} dS m^{-1} (or a relative σ change from 28.1% to 8.8%) due to the elevated ρ_b.

In the continuous liquid range ($\theta_c < \theta \le n$), electrical conduction was greatly enhanced due to the further magnified conduction in the liquid phase (Path C): a 6.7% increase in the ρ_b values caused a σ increase of 2.65–12.90 × 10^{-3} dS m^{-1} (or a relative σ change from 8.8% to 8.3%). In this range, the decrease in relative σ change might be attributed to the fact that in higher ρ_b soils, the ratios of macropores in total pore space ($1\text{-}n_{wm}/n$) are reduced, which leaves fewer continuous liquid pathways in Path C.

As mentioned previously, due to the assumption of a clear-cut differentiation of hydration water and menisci water, the σ(θ) curves generated with the unified model displayed a sharper transition between the hydration range and the menisci range, while the phenomenon did not occur in the observations (Fig. 6). Further research is required to address this issue.

4.4. Analogy between λ and σ

Prior analysis showed that for a particular soil, both λ and σ increased with increasing θ and ρ_b, but the magnitudes of λ and σ increases varied considerably within various ranges of soil water (Fig. 4). In the hydration water range (section I), λ and σ values were small and hardly changed. In the menisci water range (section II), λ increased rapidly with θ while σ increased slowly. In the continuous liquid range (section III), the increase in λ slowed down as compared to that in the menisci water range, while in contrast, σ increased exponentially with increasing θ values. These trends of λ and σ increases as a function of θ have also been reported by Hamamoto et al. (2010). It is worth noting that a hump appears in the electrical conductivity curve at the transition between the hydration range and the menisci range. This is caused by the fact that in the hydration range, electrical conduction occurs mainly through the solid pathway. As θ increases (i.e., the menisci range), however, the solid–liquid pathway contributes significantly to electrical conduction. Thus, the σ values calculated with Eq. [9] increase sharply at the transition point, because the electrical conductivity of liquid is 4–100 times greater than that of the solid.

We applied the normalization approach to quantify the relationship between the λ(θ) and σ(θ) curves. The dimensionless λ and σ values are calculated by using Eqs. [12] and [13],

$$K_e(\lambda) = \frac{\lambda - \lambda_{dry}}{\lambda_{sat} - \lambda_{dry}} \tag{12}$$

$$K_e(\sigma) = \frac{\sigma - \sigma_{dry}}{\sigma_{sat} - \sigma_{dry}} \tag{13}$$

where $K_e(\lambda)$ and $K_e(\sigma)$ are the normalized thermal conductivity and electrical conductivity; λ_{dry} and λ_{sat} represent the thermal conductivities of dry and saturated soils, respectively; σ_{dry} and σ_{sat} are the bulk electrical conductivities of dry and saturated soils, respectively. We applied Eq. [8] to calculate the λ or σ values of the dry soils, and Eq. [10] to calculate the λ or σ values of the saturated soils.

Table 2 presents the conductivity values of the sand and silt loam soils at dry and saturated conditions. For both soils, the λ_{dry} and σ_{dry} values are limited to a narrow range, while the σ_{sat} values varied significantly between soil textures and among different ρ_b treatments.

Figs. 7 and 8 show the dynamics of $K_e(\lambda)$ and $K_e(\sigma)$ results as a function of S and ρ_b. For comparison, the unified series–parallel resistor model results and the observed values are presented. Two distinct features are clear. First, $K_e(\lambda)$ and $K_e(\sigma)$ versus S can be divided into three saturation ranges (a detailed description of the trend is provided in section 4.1). In Section I, both $K_e(\lambda)$ and $K_e(\sigma)$ hardly varied due to the limited conduction pathways. As S increased (Section II), 'water bridges' developed, which enhanced the formation of solid-to-solid pathways. As a result, a sharp $K_e(\lambda)$ increase but only a slight $K_e(\sigma)$ increase were observed due to the high λ and low σ of soil solids. In Section III,

continuous liquid pathways were formed and the $K_e(\lambda)$ and $K_e(\sigma)$ responded differently to increasing S. A gradual $K_e(\lambda)$ increase was observed, while $K_e(\sigma)$ increased exponentially.

Second, for all soil textures and ρ_b values, the shapes of the $K_e(\lambda)$-S and $K_e(\sigma)$-S curves were rather symmetrical about the $y = x$ line. The same phenomenon has been reported as the "mirror image" effect for σ and λ by Revil (2000) and Hamamoto et al. (2010). In Part 2 of this study, we use the "mirror image" analogy to establish a σ model based on the λ model.

It is interesting that the modelled $K_e(\sigma)$-S curves of soils H1 and H2 were concave up in Sections II and III but concave down near the transition between Sections I and II (Fig. 7). This phenomenon results from the assumptions and simplifications in model development, which have been explained in section 4.3. In the measurements, however, the above situation occurred only for the sand soil and not for the silt loam soil (Fig. 8). Tuli and Hopmans (2004) reported similar instances. This might be related to the interaction between soil particles and adsorbed water which governs electrical conduction in the dry range. For the sand soil with low clay content, most of the adsorbed water molecules distribute on particle surfaces, which results in higher σ values than occur for the silt loam soil, due to the large number of water bridges linking sand grains. For the silt loam soil, because of its higher clay content, the adsorbed water molecules are allocated on the clay surfaces as well as inside the aggregates, and more water is required to form the same number of bridges as found in the sand soil. Thus, a concave down portion does not appear near the transition between Sections I and II for the silt loam soil.

4.5. Limitations and potential directions

In this study, the soil water status was divided into three water content ranges, and a piecewise function was applied to describe the λ and σ curves, which produced abrupt λ and σ changes at the transitional water contents because the model ignored the gradual evolution of pore size and soil structure effects on heat and electrical conductions. We propose two potential approaches that may produce continuous functions for the unified series–parallel model by addressing the gradual evolution of soil pore size distribution. First, it is essential to develop techniques that can quantify the transitional water between soil pores in the hydration, menisci, and continuous liquid ranges, which will enable a smooth transition between the three water ranges. For example, probability density functions may better describe variations of λ and σ at the inflection point. Secondly, it may be necessary to introduce the matric potential of soil water into the cubic cell model, which can characterize soil pore size distribution and the status of soil water, and the variations of λ and σ with soil water status.

5. Conclusions

In soils with a unimodal pore size distribution, the efficiency of heat and electrical conduction differ significantly in the hydration range, menisci range, and continuous liquid range. In this study, a representative cubic unit cell, that describes the λ(θ) and σ(θ) curves using an Ohm's law analogy, was introduced to evaluate the effects of soil texture and ρ_b on heat and electrical conduction through the solid, solid–liquid, and liquid pathways for various water content ranges. Model results showed that although λ and σ responded differently to soil water content, a "mirror image" phenomenon existed between the normalized thermal conductivity and electrical conductivity (i.e., $K_e(\lambda)$ and $K_e(\sigma)$). The model results generally agreed with observed values, indicating that the cubic unit cell model could be applied to quantify soil heat and electrical conduction, which could inform future studies of coupled heat and solute transfer in soils.

Declaration of Competing Interest

The authors declare that they have no known competing financial interests or personal relationships that could have appeared to influence the work reported in this paper.

Data availability

Data will be made available on request.

Acknowledgements

This research was supported by the Strategic Priority Research Program of the Chinese Academy of Sciences (XDA28010402), the National Natural Science Foundation of China (41977011), the 2115 Talent Development Program of China Agricultural University (1191-00109011), and the U.S. National Science Foundation (2037504) and USDA-NIFA Multi-State Project 4188.

Appendix A

Table A1

Appendix B

Determination of λ and σ of soil solids, air, and liquid

The λ values of liquid (λ_w) and air (λ_a) are 0.56 and 0.025 W m^{-1} K^{-1} at 20°C, and that of solids (λ_s) is 2–7.7 W m^{-1} K^{-1} for soils with various quartz contents (de Vries, 1963; Tarnawski and Leong, 2012). For hypothetical soils H1 and H2, the λ_s values are determined from their mineral compositions, i.e., the contents of quartz and other minerals following (Johansen, 1975),

$$\lambda_s = \lambda_q^q \lambda_o^{1-q} \tag{B1}$$

where λ_q and λ_o are thermal conductivities of quartz (7.7 W m^{-1} K^{-1}) and other minerals, respectively; q is the quartz content, which is assumed to be equal to the sand content. In this study, λ_o is taken as 2.0 W m^{-1} K^{-1} for soils with $q > 0.2$, and 3.0 W m^{-1} K^{-1} for soils with $q \leq 0.2$ (Johansen, 1975).

Angenheister (1982) and Palacky (1987) found σ values of solids (σ_s) for sand, loam, and clay to vary in the range of 0.001–0.025, 0.04–0.50, and 0.07–2.0, respectfully, and that of air (σ_a) was 0.0001 dS m^{-1} at 20°C. For soils with various clay contents, the σ values of liquid (σ_w) varied from 0.1 to 100 dS m^{-1} (McNeill, 1980; Palacky, 1987). In our study, σ_w values of two hypothetical soils are determined within this range, and following the fact that the presence of clay minerals increases the σ_w because of their electrically 'active' surface. Thus, for the hypothetical soils, the λ_a, λ_w, and σ_a values are set as 0.025 W m^{-1} K^{-1}, 0.56 W m^{-1} K^{-1}, and 0.0001 dS m^{-1}, respectively. The σ_s and σ_w values are set as 0.025 dS m^{-1} and 0.40 dS m^{-1} for soil H1, and 0.040 dS m^{-1} and 3.00 dS m^{-1} for soil H2 by considering clay contents.

Appendix C

Determination of side length parameters

According to Lu et al. (2007), the λ_{dry} value can be estimated from soil porosity n,

$$\lambda_{dry} = 0.51 - 0.56n \tag{C1}$$

In the unified series–parallel resistor model scheme, n is expressed as,

$$n = L_1 h + L_2 + \theta_{ads} \tag{C2}$$

By combining Eqs. [8], [C1], and [C2], a relationship among L_1, L_2 and h is obtained,

$$\lambda_{dry} = 0.51 - 0.56(L_1 h + L_2) = L_s\lambda_s + \frac{\lambda_s\lambda_a L_1}{(1-h)\lambda_a + h\lambda_s} + L_2\lambda_a \tag{C3}$$

From the model, L_s is expressed as a function of L_1 and L_2,

$$L_s = 1 - L_1 - L_2 \tag{C4}$$

Thus, Eq. [C3] is simplified as,

$$\lambda_{dry} = 0.51 - 0.56(L_1 h + L_2) = (1 - L_1 - L_2)\lambda_s + \frac{\lambda_s\lambda_a L_1}{(1-h)\lambda_a + h\lambda_s} + L_2\lambda_a \tag{C5}$$

Parameters h, L_1, L_s, and L_2 are all in the range of 0–1 and can be combined within reasonable bound constraints according to Eq. [C5]. For a specific soil,λ_{dry} is estimated from Eq. [C1] if n is known. Thus, Eq. [C5] can be expressed as,

$$\lambda_{dry} = (1 - L_1 + L_1 h - n)\lambda_s + \frac{\lambda_s\lambda_a L_1}{(1-h)\lambda_a + h\lambda_s} + (n - L_1 h)\lambda_a \tag{C6}$$

From Eq. [C6], the combination of L_1 and h within a reasonable range can be derived. Then, L_2 is estimated with Eq. [C2]. The detailed procedure used to determine the parameters is shown in Fig. C9.

Take soil H1 as an example. At a desired ρ_b, the corresponding h value is derived from Eq. [C6] and a designated L_1 value, and the values of L_2 and L_s are then estimated with Eqs. [C2] and [C4], respectively. In this study, we obtain the appropriate combinations of length parameters by considering the various ranges of n for different soil samples.

Appendix D

Change in section III λ values caused by an increase in ρ_b

In our unified series–parallel resistor model, we assume that water first fills relatively small soil pores (Path B) before entering larger pores (Path C). Thus, the λ value due to the continuous liquid pathways (Path C) contribution in section III can be expressed as,

$$\begin{aligned} \lambda &= \lambda_w L_{w2} + \lambda_a L_{a2} \\ &= \lambda_w L_{w2} + \lambda_a (L_2 - L_{w2}) \\ &= \lambda_w(\theta - \theta_{ads} - L_1 h) + \lambda_a(L_2 - \theta + \theta_{ads} + L_1 h) \end{aligned} \tag{D1}$$

At a specific water content, the λ change (Δλ) due to a change in ρ_b (ρ_{b1} and ρ_{b2}) is,

$$\Delta\lambda = \lambda_2 - \lambda_1 = (\lambda_a - \lambda_w)(L_{1-2}h_2 - L_{1-1}h_1) + \lambda_a(L_{2-2} - L_{2-1}) \tag{D2}$$

where λ_1, h_1, $L_{1\text{-}1}$, $L_{2\text{-}1}$ and λ_2, h_2, $L_{1\text{-}2}$, $L_{2\text{-}2}$ are the thermal conductivity, h, L_1, L_2 of soil at ρ_{b1} and ρ_{b2}, respectively.

Thus, it is obvious that an increase in λ caused by an increase in ρ_b at a specific θ is only related to the side length L_1, L_2, and h from Eq. [D2]. As water content increases, the side lengths of the cubic cell model remain constant at a specific ρ_b, which results in a constant λ increase occurring due to an elevated ρ_b in this range.

References

Abu-Hamdeh, N.H., Reeder, R.C., 2000. Soil thermal conductivity: effects of density, moisture, salt concentration, and organic matter. Soil Sci. Soc. Am. J. 64 (4), 1285–1290.

Angenheister, G., 1982. Physical Properties of Rocks. Springer-Verlag, Berlin.

Campbell, G.S., 1985. Soil Physics with BASIC: Transport Models for Soil-Plant Systems. Elsevier Science Publishing, New York.

Clapp, R.B., Hornberger, G.M., 1978. Empirical equations for some soil hydraulic properties. Water Resour. Res. 14 (4), 601–604.

de Vries, D.A.,1963. Physics of Plant Environment, chap. 7, ed. by W.R. van Wijk (North-Holland, Amsterdam).

Ewing, R.P., Horton, R., 2007. Thermal conductivity of a cubic lattice of spheres with capillary bridges. J. Phys. D Appl. Phys. 40 (16), 4959–4965.

Farouki, O.T., 1986. Thermal Properties of Soils. Trans Tech Publication, Switzerland.

Fragkogiannis, G., Apostolopoulos, G., Stamataki, S., 2010. Correlation of thermal conductivity and electrical resistivity of soil-for near surface geothermal applications. IEICE-Trans. Inf. Syst. E89-D (3), 1116–1119.

Hamamoto, S., Moldrup, P., Kawamoto, K., Komatsu, T., 2010. Excluded-volume expansion of Archie's law for gas and solute diffusivities and electrical and thermal conductivities in variably saturated porous media. Water Resour. Res. 46 (6), 6514.

Johansen, O., 1975. Thermal Conductivity of Soils. Norwegian University of Science and Technology, Trondheim. Ph.D. diss.

Logsdon, S.D., Green, T.R., Bonta, J.V., Seyfried, M.S., Evett, S.R., 2010. Comparison of electrical and thermal conductivities for soils from five states. Soil Sci. 175 (12), 573–578.

Lu, N., Dong, Y., 2015. Closed-form equation for thermal conductivity of unsaturated soils at room temperature. J. Geotech. Geoenviron. Eng. 141 (6), 04015016.

Lu, Y.L., Lu, S., Horton, R., Ren, T.S., 2014. An empirical model for estimating soil thermal conductivity from texture, water content, and bulk density. Soil Sci. Soc. Am. J. 78 (6), 1859–1868.

Lu, Y.L., Horton, R., Ren, T.S., 2018. Simultaneous determination of soil bulk density and water content: a heat pulse-based method. Eur. J. Soil Sci. 69 (5), 947–952.

Lu, S., Ren, T.S., Gong, Y.S., Horton, R., 2007. An improved model for predicting soil thermal conductivity from water content at room temperature. Soil Sci. Soc. Am. J. 71 (1), 8–14.

McNeill, J.D., 1980. Electrical Conductivity of Soils and Rocks. Geonics Ltd., p. 5. Technical Note.

Nadler, A., Frenkel, H., 1980. Determination of soil solution electrical conductivity from bulk soil electrical conductivity measurements by the four-electrode method. Soil Sci. Soc. Am. J. 44 (6), 1216–1221.
Nouveau, M., Grandjean, G., Leroy, P., Philippe, M., Hedri, E., Boukcim, H., 2016. Electrical and thermal behavior of unsaturated soils: experimental results. J. Appl. Geophys. 128, 115–122.
Palacky, G., 1987. Resistivity characteristics of geologic targets. Electromagnetic methods. Appl. Geophys. 1.
Revil, A., 2000. Thermal conductivity of unconsolidated sediments with geophysical applications. J. Geophys. Res. 105 (B7), 16749–16768.
Rhoades, J.D., Manteghi, N.A., Shouse, P.J., Alves, W.J., 1989. Soil electrical conductivity and soil salinity: new formulations and calibrations. Soil Sci. Soc. Am. J. 53 (2), 433–439.
Singh, D.N., Kuriyan, S.J., Manthena, K.C., 2001. A generalized relationship between soil electrical and thermal resistivities. Exp. Therm Fluid Sci. 25 (3–4), 175–181.
Sreedeep, S., Reshma, A.C., Singh, D.N., 2005. Generalized relationship for determining soil electrical resistivity from its thermal resistivity. Exp. Therm. Fluid Sci. 29 (2), 217–226.
Stadler, A., Rudolph, S., Kupisch, M., Langensiepen, M., Kruk, J., Ewert, F., 2015. Quantifying the effects of soil variability on crop growth using apparent soil electrical conductivity measurements. Eur. J. Agron. 64, 8–20.
Sudduth, K.A., Kitchen, N.R., Wiebold, W.J., Batchelor, W.D., Bollero, G.A., Bullock, D. G., Clay, D.E., Palm, H.L., Pierce, F.J., Schuler, R.T., Thelen, K.D., 2005. Relating apparent electrical conductivity to soil properties across the north-central USA. Comput. Electron. Agric. 46 (1–3), 263–283.
Sun, Q., Lü, C., 2019. Semi-empirical correlation between thermal conductivity and electrical resistivity for silt and silty clay soils. Geophysics 84 (3), MR99–MR105.
Tarnawski, V.R., Leong, W.H., 2012. A series-parallel model for estimating the thermal conductivity of unsaturated soils. Int. J. Thermophys. 33 (7), 1191–1218.
Tokoro, T., Ishikawa, T., Shirai, S., Nakamura, T., 2016. Estimation methods for thermal conductivity of sandy soil with electrical characteristics. Soils Found. 56 (5), 927–936.
Tuli, A., Hopmans, J.W., 2004. Effect of degree of fluid saturation on transport coefficients in disturbed soils. Eur. J. Soil Sci. 55 (1), 147–164.
Wang, J., Zhang, X., Du, L., 2017. A laboratory study of the correlation between the thermal conductivity and electrical resistivity of soil. J. Appl. Geophys. 145, 12–16.
Woodside, W., Messmer, J.H., 1961. Thermal conductivity of porous media. 1. unconsolidated sands. J. Appl. Phys. 32 (9), 1688.